# Activation of two dopants, Bi and Er in $\delta$ -doped layer in Si crystal

Koichi Murata<sup>†</sup>, <sup>1, 2, \*</sup> Shuhei Yagi, <sup>1, 3, †</sup> Takashi Kanazawa, <sup>1, 2</sup> Satoshi Tsubomatsu, <sup>1, 2</sup>
Christopher Kirkham, <sup>1, 4, 5</sup> Koh-ichi Nittoh, <sup>1</sup> David R. Bowler, <sup>1, 4</sup> and Kazushi Miki<sup>1, 2, 6, ‡</sup>

<sup>1</sup> National Institute for Materials Science (NIMS),

Namiki 1-1, Tsukuba, 305-0044, Japan

<sup>2</sup> Faculty of Pure and Applied Sciences, University of Tsukuba,

Tennodai 1-1-1, Tsukuba, 305-8573, Japan

<sup>3</sup> Graduate School of Science and Engineering,

Saitama University, 255 Shimo-Okubo, Sakura-ku,

Saitama City, Saitama, 338-8570, Japan

<sup>4</sup> London Centre for Nanotechnology, University College London,

Gower Street, London WC1E 6BT, UK

<sup>5</sup> Center for Computational Sciences, University of Tsukuba,

Tennodai 1-1-1, Tsukuba, 305-8577, Japan

<sup>6</sup> Department of Electrical Materials and Engineering,

University of Hyogo, Shosya 2167, Himeji, Hyogo, 671-2280, Japan

# Abstract

Conventional doping processes are no longer viable for realizing extreme structures, such as a  $\delta$ -doped layer with multiple elements, such as the heavy Bi, within the silicon crystal. Here, we demonstrate the formation of (Bi+Er)- $\delta$ -doped layer based on surface nanostructures, i.e. Bi nanolines, as the dopant source by molecular beam epitaxy. The concentration of both Er and Bi dopants is controlled by adjusting the amount of deposited Er atoms, the growth temperature during Si capping and surfactant techniques. Subsequent post-annealing processing is essential in this doping technique to obtain activated dopants in the  $\delta$ -doped layer. Electric transport measurement and photoluminescence study revealed that both Bi and Er dopants were activated after post-annealing at moderate temperature.

<sup>\*</sup> m-koichi@criepi.denken.or.jp; Current address: Central Research Institute of Electric Power Industry,

<sup>2-6-1</sup> Nagasaka, Yokosuka, Kanagawa, 240-0196, Japan

<sup>&</sup>lt;sup>†</sup> These two authors contributed equally.

<sup>&</sup>lt;sup>‡</sup> miki@eng.u-hyogo.ac.jp

#### I. INTRODUCTION

Co-doping techniques, doping of multiple elements into host materials, are available for a variety of growth techniques, including bulk crystal growth, thin film epitaxial growth and ion implantation[1]. These techniques are often used for various purposes such as: counterdoping, to obtain semi-insulating layers, engineering the band structure of semiconductors based on two compounds, e.g. InAs and GaAs for  $In_xGa_{1-x}As$ , and buffering the lattice strain in the crystal, which is often induced by incorporating elements with large atomic radii. As for co-doping in silicon (Si) crystal, it seems there are no reports studying electronic states of multiple dopants, i.e. regarding dopant activation, towards applications although there are a few reports on structural aspects [2, 3]. Since Si technology has been developed along complementary metal-oxide-semiconductors (CMOS) for Large Scale Integration (LSI), mostly III or V group elements have been studied. To go beyond current LSI technology, a novel information processing platform is required, such as quantum information processing platforms (QIPs). One approach for realizing scalable QIP has been proposed using localized electron spins bound by donors in the Si crystal. To date, spin ensemble properties have been studied, and their control has been demonstrated [4, 5]. The next stage is manipulation of single spins, which is still an unsolved problem, related to limitations of the structural implementations. As a solution, a Bi- $\delta$ -doped layer with a density of around 0.01 nm<sup>-2</sup> could be ideal [6]. Atomic scale manipulation of Bi atoms in Si has been recently demonstrated using an electron beam [7]. According to the Stoneham proposal, Er atoms can be used as a control gate for Bi atoms by optical excitation [6]. However, conventional doping techniques cannot precisely place two different elements into a nm-thick layer. Although III and V-group elements, except Bi, are well studied as dopants in Si crystal, there is plenty of room for the study of other elements as dopants for unrealized novel information platforms.

Beyond the limitations of conventional doping techniques, we focus on a doping technique based on surface engineering, with Bi nanolines (NLs) [3, 8] as dopant sources. The Bi NL consists of two parallel rows of Bi dimers with 5-7-5 membered rings of Si, named the Haiku core, underneath [9]. Since this is more stable than Bi  $(2 \times n)$ , the surface segregation problem can be avoided, resulting in a  $\delta$ -doped profile [3]. In a previous study, an autosurfactant technique for Bi doping in Si crystal has been demonstrated, which enables us to

realize a highly-concentrated Bi  $\delta$ -doped layer by molecular beam epitaxy (MBE) [10]. Even during surfactant-free-growth (SFG), some Bi atoms in Bi NLs remain at the initial layer underneath a Si capping layer. This doping technique using Bi NLs can be extended to codoping with a 2nd element, which is the thesis of this study. This concept has been partially demonstrated by the formation of (Bi+Sb)- $\delta$ -doped layer in Si, formed by depositing a Sb surfactant layer atop the Bi NLs prior to the Si capping layer growth [3]. Note that scanning tunneling microscopy (STM) based studies revealed unique interactions between Bi NLs and deposited 2nd elements such as In and Ag [11].

In this work, we demonstrate a method to create a (Bi+Er)- $\delta$ -doped layer in Si crystal by using MBE. The secondary ion mass spectrometry (SIMS) analysis reveals that the density of Er atoms in the  $\delta$ -doped layer can be controlled by adjusting the amount of deposited Er atoms on the Bi NL covered surface. The density of Bi atoms in the  $\delta$ -doped layer can be tuned by the growth temperature during Si capping, as well as the coverage of the Bi surfactant layer. Electrical transport measurement address the activation of Bi dopants in the  $\delta$ -doped layer, which is supported by comprehensive DFT calculations regarding the thermal stability of the layer. The photoluminescence study proves the electronic state of Er dopants in Si. Considering both properties of Bi-doped and Er-doped layers, we shall show that the activation of both Bi and Er dopants can be achieved simultaneously by post-annealing at moderate temperature after MBE growth.

## II. EXPERIMENT

All samples were grown by an ion-pumped Si MBE system with an electron-beam evaporator for Si growth and a resistively-heated effusion cell for the evaporation of Bi and Er. The base pressure was typically  $2 \times 10^{-7}$  Pa. The growth rate of Si was 15 Å/min. Bi and Er fluxes were  $3 \times 10^{12}$  and  $1 \times 10^{12}$  atoms cm<sup>-2</sup>s<sup>-1</sup>, respectively. Deposited amounts of Bi and Er atoms were estimated by the deposition time based on the fluxes. A 20 keV reflection high-energy electron diffraction (RHEED) system was used for monitoring surface structures. A highly resistive Si(001) substrate was subjected to a standard cleaning process[12]. In the growth chamber, a chemically formed oxide layer was desorbed by heating with Si flux to establish an Si(001)  $2 \times 1$  surface. As buffer layer, 100 nm-thick Si epitaxial layer was grown. Whilst maintaining the substrate temperature at around  $600^{\circ}$ C, the surface was exgrown.

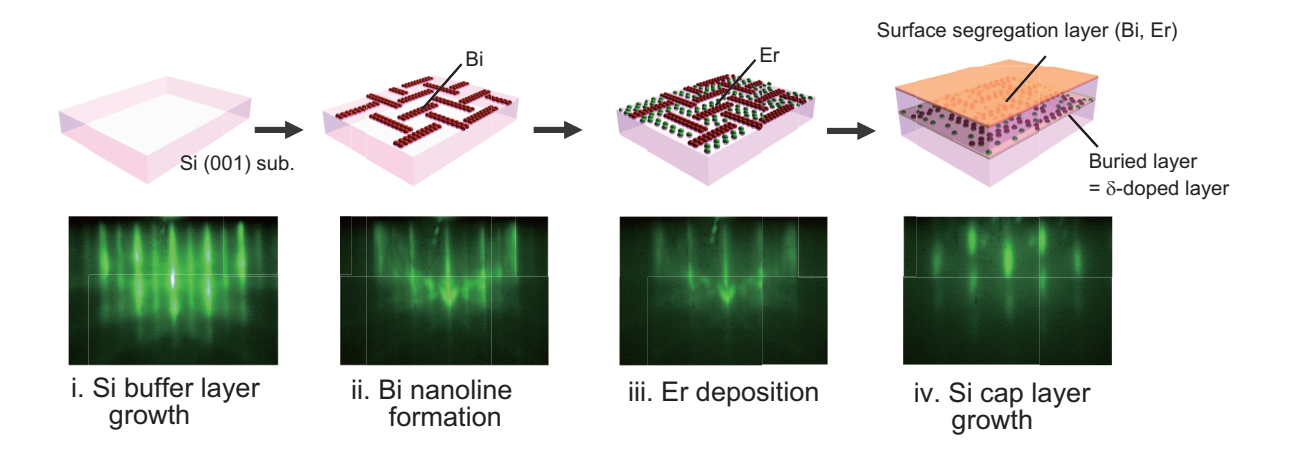


FIG. 1. Schematic illustration of formation of (Bi+Er)- $\delta$ -doped layer in Si crystal with RHEED patterns (from [1 $\overline{1}0$ ] direction). i. clean Si(001) surface exhibiting (2 × 1) RHEED pattern. ii. Bi NLs form on Si(001) surface by depositing Bi atoms, showing signature 1D pattern (circular arc). iii. Er atoms (2nd dopant) are deposited on the surface with Bi NLs, reducing the intensity of RHEED pattern. iv. Si cap layer was epitaxially grown  $\delta$ -doped layer with Bi and Er remaining at the original depth.

posed to a Bi flux in order to create Bi NLs, showing one-dimensional RHEED patterns [8]. The substrate temperature was then ramped down to < 440°C and the desired amount of Er was deposited. Finally a 50 or 100 nm-thick Si cap layer was grown.

For electrical measurements, different cleaning methods were adopted to suppress unintentional counter-doping, such as B. Prior to loading into the growth chamber, 1% DHF (Diluted hydrogen fluoride) was spin-coated in an Ar atmosphere to etch the protective oxide layer [12]. Since the target layer is dilute in this study, and should be n-type, it is important to reduce the background doping level, especially p-type dopants. The substrate was then immediately loaded into the growth chamber. A RHEED pattern corresponding to a H-terminated Si(001)  $1 \times 1$  surface was observed without any heating. Thermal annealing at  $800^{\circ}$ C desorbed the H atoms to establish an Si(001)  $2 \times 1$  surface. Further processing was as above. Instead of crystalline Si, an amorphous Si capping layer was deposited at around room temperature.

After MBE growth, the sample was diced into small pieces and the surface layer was chemically etched-off [13]. Furnace annealing (QHC-P410CP; ULVAC-RIKO) was carried

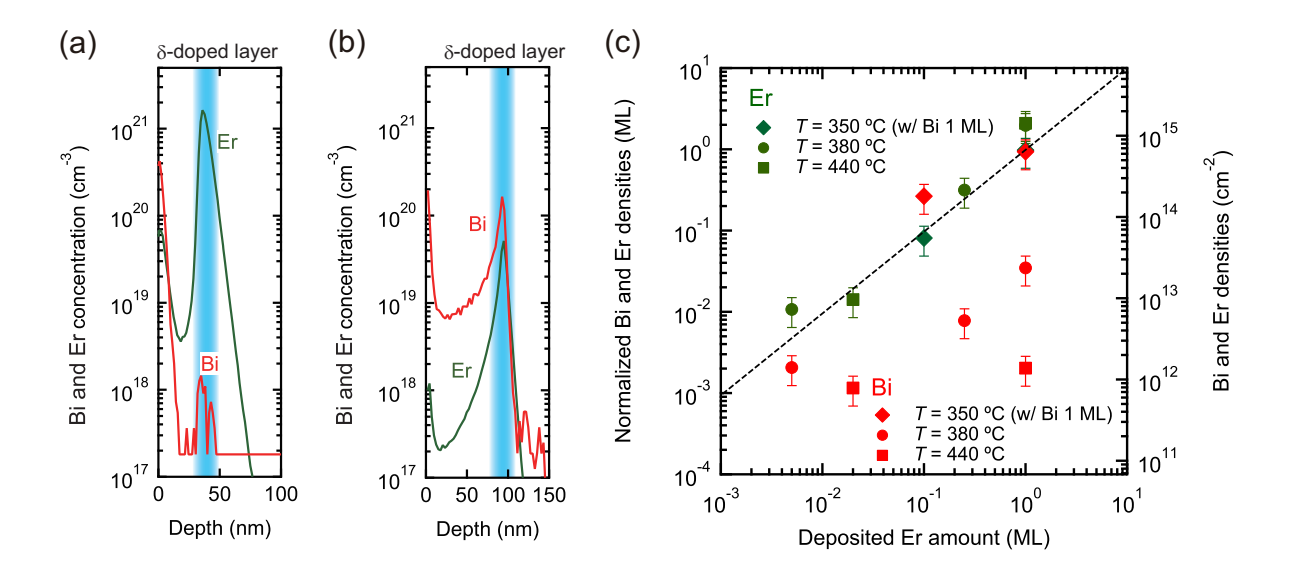


FIG. 2. Depth profiles of Bi and Er concentrations in Si crystal for (a) deposition of 1ML of Er and growth at 440°C and (b) deposition of 0.1 ML of Er and growth at 350°C with 1 ML of Bi surfactant. (c) Bi and Er densities in the  $\delta$ -doped layer as function of deposited Er amount. The dashed line with slope = 1 was inserted as visual guide.

out at various temperatures in ambient nitrogen as a post-annealing process. Photoluminescence (PL) was recorded by using a low-power CW 532-nm DPSS laser as an excitation source and a grating monochromator (HR320; Jobin Yvon) equipped with a cooled Ge infrared photo-detector (North Coast Scientific). For electrical transport measurements, the specimens were fabricated into the Hall-bar structure  $(70\times600~\mu\text{m}^2)$  by standard microfabrication techniques. Deep contact holes were opened by dry etching before the deposition of 200 nm-thick Al films for electrodes. Finally, the specimens were annealed at 400°C in Ar +  $\text{H}_2(3\%)$  for 10 min. Electrical measurements were carried out by the four-terminal geometry using the probe station (TKS-MP-V300-20mm; Toei Scientific Industrial Co., Ltd) with Semiconductor Analyzer (B1500A; Agilent Technology). Structural analysis was carried out by transmission electron microscopy (TEM)(JEM 2100F; JEOL) and secondary ion mass spectrometry(SIMS)(IMS-7f; CAMECA).

Calculations were performed using density functional theory (DFT) [14, 15], as implemented in the Vienna *Ab initio* Simulation Package (VASP) [16, 17]. The core electrons were described by the projector augmented wave (PAW) method, [18, 19] with the gradient

corrected Perdew-Burke-Ernzerhof (PBE) exchange-correlation functional [20]. For Bi, the  $6s^26p^3$  electrons were treated as valence, the rest as core. An energy cut-off of 300 eV was used, with a  $2\times2\times2$  Monkhorst-Pack k-point mesh. All calculations were spin polarized, with no restrictions placed on the spins. A 512 atom bulk Si cell was used throughout, with a calculated theoretical lattice constant of 5.469 Å. We considered two types of diffusion for Bi in bulk Si, either vacancy mediated or not. In both cases one Si atom was replaced with a substitutional Bi. In the former case we also created a variety of single Si vacancies located at the nearest to fourth nearest site from the Bi atom. All atoms were allowed to relax until a 0.02 eV/Å convergence condition for the forces on each atom was reached. We used the Climbing Image Nudged Elastic Band (CINEB) method [21] to calculate the diffusion barriers for a variety of diffusion routes. We considered diffusion between equivalent end points, with the position of the Bi atom swapped with another feature; a vacancy for vacancy mediated, and a Si atom otherwise.

#### III. RESULTS AND DISCUSSION

## A. (Bi+Er) $\delta$ -doping

A schematic illustration of the concept of (Bi+Er)  $\delta$ -doping is shown in Fig. 1 with typical RHEED patterns (from <110>direction) during the growth. Here 1 ML is defined as  $6.8 \times 10^{14}$  cm<sup>-2</sup> for the Si(001) surface. The clean Si(001) surface exhibits a half streak pattern which reflects the 2×1 surface (i). A unique one-dimensional circular arc within the half streak pattern appears after the formation of Bi NLs, which are superimposed, resulting in chevron patterns (ii). By depositing sub-ML Er on the Bi NL covered surface, the intensity of the RHEED pattern reduces, in particular the half streak (iii). Since the circular pattern remains, this suggests most Er is deposited not on Bi NLs. We estimate the chance of Bi and Er atoms encountering each other at only 1% since their densities are 1/8 ML and 0.1 ML, respectively. Note that the interaction between Bi and Er atoms might be necessary to consider when Er amount is close to 1 ML. Finally epitaxial growth of Si cap layer results in a slightly spotty 2D pattern, indicating a rougher surface, due to the relatively low temperature growth and the existence of the surface segregation layer (iv). As mentioned above, most Bi atoms rise towards the surface due to the surface segregation.

Figure 2(a) and (b) show depth profiles of Bi and Er atoms in Si crystal, which is obtained by SIMS analysis, with the position of  $\delta$ -doped layers highlighted. In Fig. 2(a), 1 ML of Er was deposited on the Bi NL covered surface, and a 50 nm-thick Si cap layer was subsequently grown at 440°C. Depth of zero represents the sample surface and non-zero densities reflect the existence of a segregation layer on the surface. Few Bi atoms and most Er atoms remained at their original position. The left side (surface side) of Er concentration profile is steeper than the right side, due to the nocking effect during SIMS analysis which broadens the width of the Er peak. The Bi and Er densities in the  $\delta$ -doped layer were  $1.4 \times 10^{12}$ and  $1.4 \times 10^{15}$  cm<sup>-2</sup>, respectively. Accounting for the controllability for deposition and the accuracy of SIMS analysis, the Er density in the  $\delta$ -doped layer matches that deposited on the surface. Whereas, the Bi density is about 0.002 ML, less than 2% of the original Bi density (1/8 ML), in good agreement prior Bi  $\delta$ -doping [10], suggesting Bi density can be controlled by auto-surfactant techniques (surface-segregation quencher). Bi and Er depth profiles, with a Bi surfactant are shown in Fig. 2(b), which was grown with 1 ML of Bi surfactant after Er deposition (0.1 ML) at 350°C. The thickness of the Si cap layer was 100 nm. In contrast to Fig. 2(a), the distributions of Bi and Er atoms in Fig. 2(b) would reflect more real due to less influence of the knocking effect. The Bi and Er densities in the  $\delta$ -doped layer were  $1.8 \times 10^{14}$  and  $5.5 \times 10^{13}$  cm<sup>-2</sup>, respectively. The Bi density in the  $\delta$ -doped layer stayed at the density of initial Bi NLs, which demonstrates the usefulness of the Bi auto-surfactant technique for (Bi+Er)  $\delta$ -doping as well. It should be mentioned that the coverage of the surfactant layer can control the Bi density in the  $\delta$ -doped layer, which is a part of auto-surfactant action[10].

The Bi and Er densities in  $\delta$ -doped layers in samples grown with different Er amounts (0.05 to 1 ML) at several growth temperatures (380 and 440°C) for Si cap layer is summarized in Fig. 2(c). Results for the 1 ML of Bi surfactant layer is also plotted. As seen in Fig. 2(a), the Er density increased with the amount of deposited Er. Hence, the Er density in the  $\delta$ -doped layer is controlled by adjusting the initial amount of Er deposited. It has been reported that the surface segregation of Er atoms is kinetically-limited below 550°C [22], which agrees well with present results. On the other hand, the Bi density in the  $\delta$ -doped layer decreased with increasing growth temperature, due to the strong tendency for surface segregation of Bi atoms [10, 23]. Furthermore, the Bi density increased with increased deposited Er. The Er atoms act as an effective surfactant in kinetically-limited growth,

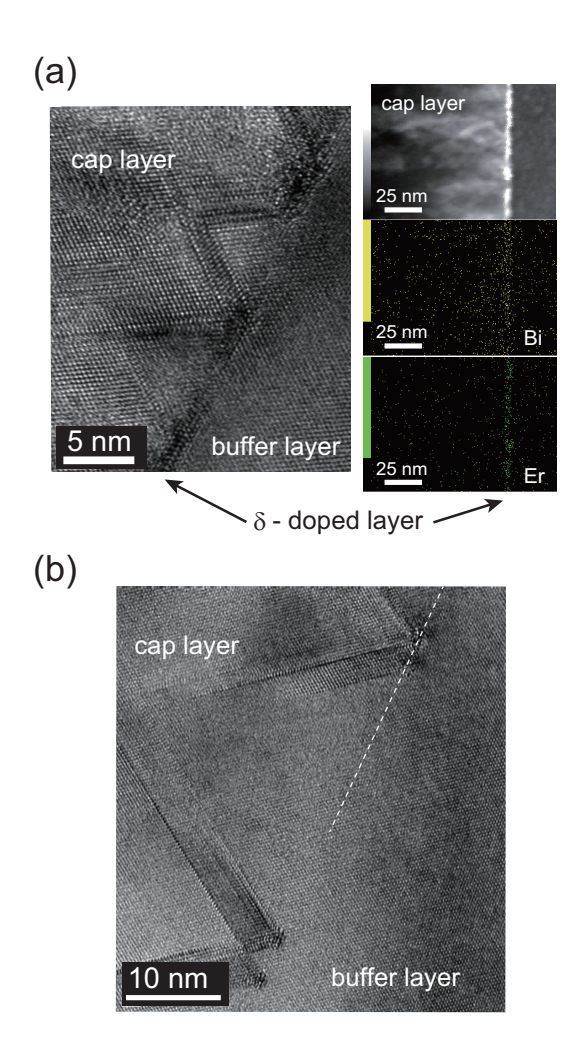


FIG. 3. Cross-sectional views of (Bi+Er)- $\delta$ -doped samples with Er (a) 1 ML and (b) 0.1 ML, grown with 1 ML of Bi surfactant layer. The right hand images in (a) are HAADF-STEM (High-angle Annular Dark Field Scanning TEM) images with Energy dispersive X-ray spectroscopy (EDS) mappings for Bi and Er, respectively. The dashed line in (b) indicates the possible location of the  $\delta$ -doped layer.

preventing Bi-Si exchange. As an extreme case, a  $\delta$ -doped layer with 1 ML Er, and a 1 ML Bi surfactant layer was grown and the Bi density in the  $\delta$ -doped layer was about 1 ML implying the Bi surfactant layer did not rise because of incomplete of epitaxial growth.

Figure 3 shows the cross-sectional views of (Bi+Er)-δ-doped samples with Er of (a) 1 ML and (b) 0.1 ML using Bi 1 ML surfactant. The right hand side of Fig. 3(a) shows the HAADF-STEM(High-angle Annular Dark Field Scanning TEM) images with Bi and Er

mapping, showing the  $\delta$ -doped layer consists of the heavy elements Bi and Er. Note that bright spots in cap and buffer layers would be artifacts due to the sensitivity and signal to noise ratio in current EDS mapping. Whereas, the  $\delta$ -doped layer is not visible in (b), with the possible location indicated by a dashed line. It should also be noted that the Si cap layer of (a) is polycrystalline, whilst (b) has a high-quality epitaxial layer. Previous TEM studies showed that Bi is the origin of the lattice defects in Si cap layer[24]. Hence,  $\delta$ -doping with sub-ML of Er atoms is essential in this method. To generalize, the growth conditions for the  $\delta$ -doped layer would be need to be adjusted, depending on the surface segregation tendency of the atoms involved.

# B. Towards activation of Bi and Er dopants

The (Bi+Er)- $\delta$ -doped layer was structurally realized in subsection A. It must still be determined whether the Bi and Er dopants are electrically / optically activated or not. From fundamental physics, Bi should be an n-type dopant, whose donor level,  $E_D = 69 \text{ meV}$ , is below the conduction band edge of Si [25]. Previous photoluminescence study revealed the development of a Bi donor band after high temperature annealing [26]. However, the necessity of the annealing process for dopant activation is not fully understood.

The local arrangement of activated Er atoms is complex. Optically activated Er atoms are surrounded by six-fold O atoms and the intra-shell transition of Er<sup>3+</sup> ion emits photons of 806 meV [27]. Co-doping with O has attracted attention to gain enhanced luminescence, and the formation of an Er:O complex is essential [28]. The luminescence mechanism is considered as energy transfer from the host material via the Er-related trap level (e.g.  $E_T = 150$  meV, corresponding to the dominant Er-O trap state) [29, 30]. It has been reported that post-annealing at temperatures in excess of 650°C is required to initiate the formation of Er-O clusters. In the case of an Er ion implanted layer (1 MeV, 1 × 10<sup>13</sup> cm<sup>-2</sup>), the luminescence from Er<sup>3+</sup> was successfully observed after annealing at 1100°C for 30 min [31]. Higher temperature annealing can produce aggregations of Er atoms or optically inactive silicides.

For these reasons, post-annealing at certain temperature would be necessary to activate both Bi and Er dopants in the (Bi+Er)- $\delta$ -doped layer. Since Er atoms are also implicated in the formation of shallow donors in Si, it is not easy to consider the activation of Bi and

Er dopants simultaneously. Thus the post-annealing behaviour for Bi and Er dopants was investigated separately as follows.

## 1. Electrically activated Bi atoms

Because of the sub-ML Bi-doped layer, extrinsic side-effects such as unintentional doping hinder the true transport properties. In fact, an as-grown Bi  $\delta$ -doped layer (Si cap layer grown at 350°C with 1 ML of Bi surfactant layer) showed n-type doping (4×10<sup>13</sup> cm<sup>-2</sup>), which is qualitatively in agreement with the structural properties of buried Bi NLs using X-ray absorption fine structure (XAFS) techniques at the synchrotron radiation facility, SPring-8 [32]. The measured Bi-Si bond length is  $2.63 \pm 0.02$  Å in the Bi  $\delta$ -doped layer capped by Si crystal, which is shorter than the initial value of  $2.79 \pm 0.01$  Å in the Haiku structure on the surface, suggesting the Bi NLs can break up due to Si deposition. These facts suggest Bi dopants in the  $\delta$ -doped layer are electrically activated, which seems inconsistent with the non-appearing Bi-related peak on the PL spectra. To address whether Bi dopants are activated or not, a Bi  $\delta$ -doped layer beneath a Si cap layer deposited at room temperature was grown, inspired by XAFS results showing the possibility of breaking up Bi NLs [32].

Figure 4(a) shows transmission electron microscope (TEM) images and RHEED patterns of Bi NLs buried beneath an amorphous Si (a-Si) layer after annealing at (i-1, i-2) 400 and (ii-1, ii-2) 500°C for 24 hours. In the latter case, the RHEED pattern of the Si(001) 2×1 surface is observed, a clear sign of recrystallization of the interfacial a-Si layer. According to the literature [33], only 1 nm of crystalline Si (c-Si) forms after 24 hours of annealing at 400°C, whereas annealing at 500°C or above transforms the entire a-Si region by solid phase epitaxial (SPE) growth. We note that Song et al. recently reported that the Haiku core (reconstructed structure beneath Bi dimers) persists even after Si cap at room temperature and SPE growth [34].

The SIMS profile of the Bi  $\delta$ -doped layer in Si after annealing at 400, 500 and 600°C in vacuum for 24 hours are shown in Fig. 4(b). Since a 50 nm-thick layer of SiO<sub>2</sub> was deposited on top of the sample by sputtering, the surface of the NLs region is actually at a depth of 50 nm. From these SIMS profiles, the location of the  $\delta$ -doped layer is clearly shown, with sharp peaks around a depth of 150 nm for each.

Simultaneously with SPE growth, Bi atoms diffused towards to surface due to surface

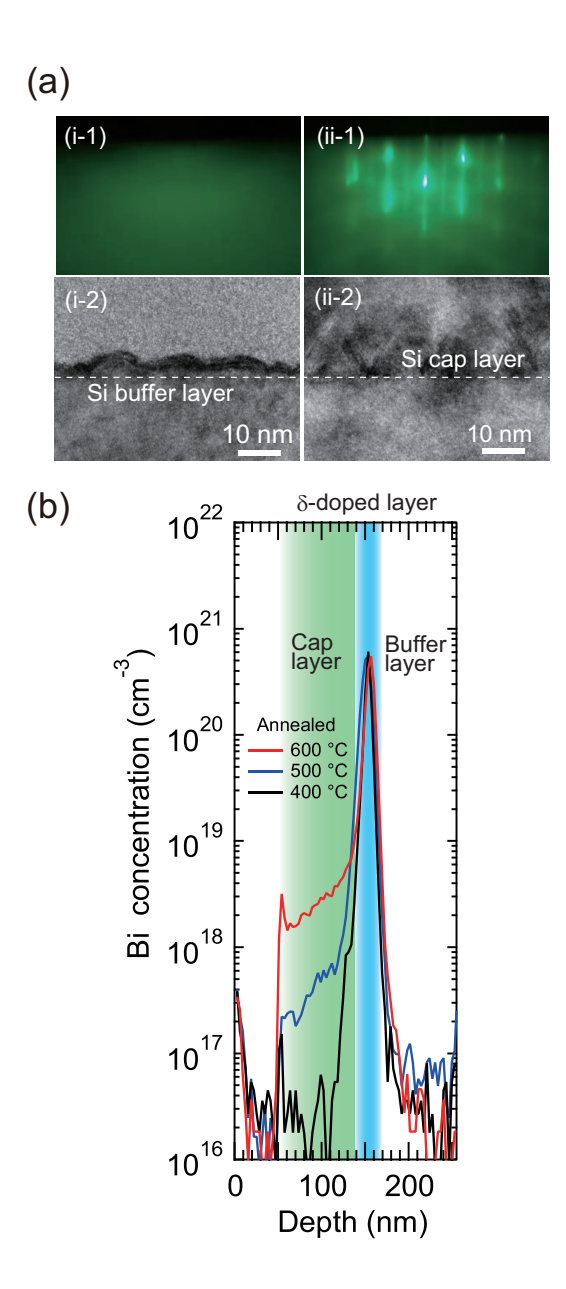


FIG. 4. (a) Cross-sectional TEM images of the Bi  $\delta$ -doped layer and the RHEED patterns from the sample surface after anneals at (i-1, i-2) 400°C and (ii-1, ii-2) 500°C. (b) SIMS profiles of the Bi  $\delta$ -doped layer after annealing in vacuum for 24 hours.

segregation phenomena, as indicated by the smaller concentrations in the NLs region. By integration of the Bi profile, the amounts of diffused Bi atoms are  $8.9 \times 10^{11}$ ,  $2.6 \times 10^{12}$  and  $2.2 \times 10^{13}$  cm<sup>-2</sup> in the samples annealed at 400, 500 and 600°C, respectively. Meanwhile the amount in the Bi  $\delta$ -doped layer is  $\sim 5 \times 10^{14}$  cm<sup>-2</sup> in all samples. This means that the

TABLE I. Carrier density and mobility of the Bi  $\delta$ -doped layer after annealing in vacuum for 24 h. Sample Nos. (A)-(D) are identical to the samples in Fig. 4(a)

| Sample No. | Structure                             | Anneal (°C) | Carrier density $p_{2D} - n_{2D}$ (cm <sup>-2</sup> | Nobility $ \mu (\text{cm}^2/\text{V}\cdot\text{s})$ |
|------------|---------------------------------------|-------------|---|---|
| (A)        | a-Si / Bi NLs                         | -           | $+\ 1\times10^{12}$                                 | $1\times10^2$                                       |
| (B)        | a-Si / Bi NLs                         | 400         | - $1 \times 10^{15}$                                | $3\times10^1$                                       |
| (C)        | a-Si / Bi NLs                         | 500         | $-3 \times 10^{14}$                                 | $3\times10^1$                                       |
| (D)        | a-Si / Bi NLs                         | 600         | $-9 \times 10^{14}$                                 | $3\times10^1$                                       |
| (E)        | a-Si / Bi NLs                         | 700         | $+\ 3\times10^{13}$                                 | $6\times10^1$                                       |
| (F)        | a-Si / Bi $(2 \times n) 1 \text{ ML}$ | -           | - $3 \times 10^{12}$                                | $2\times10^2$                                       |

amount of diffused Bi atoms are two to three orders of magnitude lower than that of the Bi  $\delta$ -doped layer. From an Arrhenius plot of the amount of diffused Bi atoms as a function of annealing temperature, an activation energy  $(E_a)$  of  $0.8 \pm 0.2$  eV was extracted. This is smaller than that of typical impurities in the Si crystal [25]. As a reference, Ishikawa *et al.* proposed that the activation energy for Bi diffusion in Si was 2.50 eV at 1050-1200°C, and occurred via a vacancy mediated diffusion model [35].

To attempt to address the situation, we performed DFT calculations for several likely diffusion routes for substitutional Bi within the Si crystal. Diffusion processes are typically expressed by the equation,  $D \sim \nu \exp\left(-\frac{\Delta E}{kT}\right)$ . Where D is a diffusion constant,  $\nu$  is the Debye frequency,  $\Delta E$  is the energy barrier, k is the Boltzmann constant, and T is the temperature. We determined  $\Delta E$  via DFT calculations of Bi diffusion in the Si crystal.

Calculations involving the exchange of Bi and Si atoms in the absence of vacancies were unsuccessful. This suggests either very high barriers, or that without vacancies there is not enough space for Bi exchange to occur. For vacancy mediated diffusion we considered four different situations, with the vacancy somewhere between the nearest and fourth nearest lattice site. We found very low barriers for diffusion to the nearest vacancy site, of only  $0.03\,\mathrm{eV}$ . However, in this scenario the Bi atom is likely to just diffuse back and forth in a small region of the crystal, rather than diffusing through the crystal. When we optimized the structure of the next nearest vacancy site it would relax to the nearest vacancy site, so no diffusion calculations were necessary. For the third and fourth nearest vacancies we found barriers of around 3 and 5 eV, respectively. The difference in these barriers is likely

due to the degree of lattice distortion as the Bi atom moves through the crystal. Our value for the third nearest vacancy of 3 eV is very close the reported values for Bi in Si [35], and supports the idea that substitutional Bi will participate in vacancy mediated diffusion.

These results suggest that Bi diffusion can be divided into two scenarios, depending on the position of vacancies relative to the Bi atoms. If there are no vacancies, or only distant vacancies, then for the temperature range of the present experiment (400 - 600°C), the barriers are too high, and diffusion will not occur. This is consistent with our experimental result, that the distribution of the  $\delta$ -doped layer is maintained, even after annealing at 600°C for 24 hours. If instead vacancies are adjacent to the Bi atoms, then diffusion can occur, but only over a very small range. This process could happen in concert with the diffusion of Si vacancies, which have barriers in the range of 0.2-2.2 eV [36], allowing some Bi to leave the  $\delta$ -doped layer during recrystallization. Therefore, we suggest that the majority of Bi atoms are immobile during the annealing process, with the small amount of diffused Bi due to nearby vacancies prior to annealing.

By measuring the Hall resistance  $R_{xy}$  as a function of external magnetic flux density B(T), we estimated the carrier density according to  $R_{xy} = R_H \cdot B/t = B/e(p_{2D} - n_{2D})$ , where  $R_H$  and t are the Hall coefficient and thickness of the specimen, respectively. Sheet (2D) carrier densities  $p_{2D}$  or  $n_{2D}$  were used rather than 3D carrier densities in this study. Without annealing, we estimated the carrier density of our sample to be  $p_{2D} - n_{2D} = +1 \times 10^{12}$  cm<sup>-2</sup>. This suggests that the Bi atoms are not at substitutional sites, and do not act as donors in the as-grown sample. This feature is consistent with our earlier XAFS results [32], which found that the Bi-Si bond length for the as-grown sample was longer than that of substitutional Bi.

Carrier densities and mobilities of samples annealed at between 400 and 700°C for 24 hours were determined and summarized in Table I. By annealing at 400°C, the carrier type changed from p to n and the carrier density reached  $\sim 10^{15}$  cm<sup>-2</sup> and the mobility dropped lower than 50 cm<sup>2</sup>/V·s. The literature on the donor density dependence of mobility in n-type Si [37], indicates that the mobility drops below 100 cm<sup>2</sup>V<sup>-1</sup>s<sup>-1</sup> when donor density is higher than  $10^{20}$  cm<sup>-3</sup>. If we assume that the thickness of the  $\delta$ -doped layer is  $\sim 20$  nm, then the 3D carrier density is  $5 \times 10^{20}$  cm<sup>-3</sup>. This corresponds to the peak in Bi concentration in the SIMS profiles (Fig. 4(b)). This indicates that the transport properties are a reflection of the Bi  $\delta$ -doped layer. In addition, carrier density remains approximately constant up to

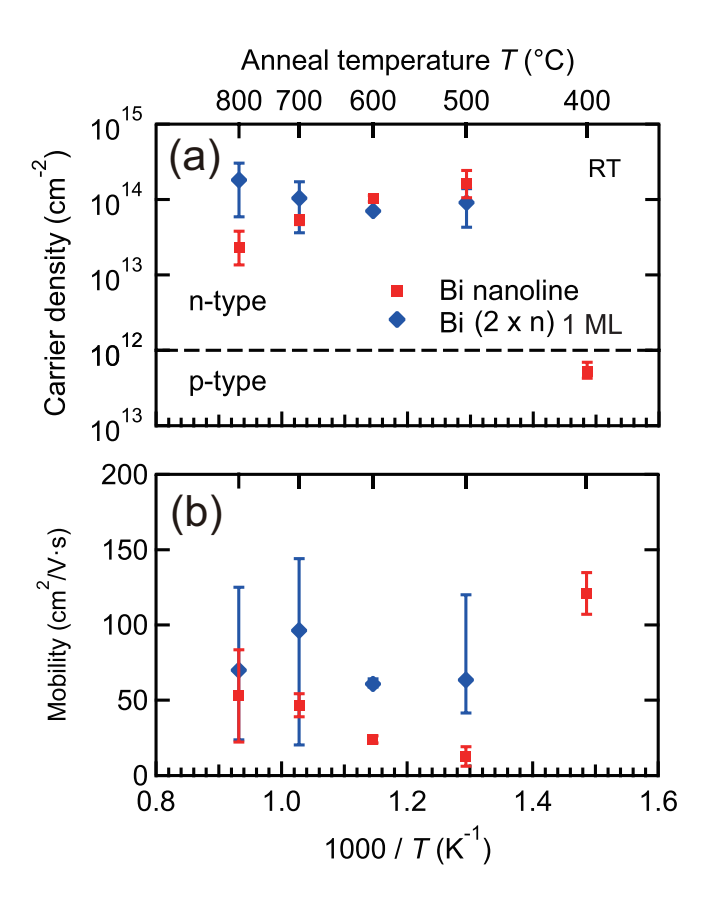


FIG. 5. Annealing temperature dependence of (a) the carrier density and (b) the mobility of the Bi  $\delta$ -doped layer. Each sample was annealed in N<sub>2</sub> ambient for 30 min. Error bars indicate maximum and minimum values obtained in the measurement for multiple samples.

600°C. After annealing at 700°C for 24 hours, remarkably the carrier type became p-type and the carrier densities decreased to  $3\times10^{13}$  cm<sup>-2</sup>.

Similar phenomena has been reported in Bi ion implanted Si [38, 39], where it should be noted that a subsequent thermal anneal is required to recover the crystalline structure and drive the dopants into the Si lattice. The electrical activation yield (EAY) of implanted Bi ions  $(5 \times 10^{14} \,\mathrm{cm}^{-2})$  is maximized by annealing at around 600°C, with annealing at higher temperatures causing it to drop [40]. On the other hand, the EAY of lightly implanted  $(1.1 \times 10^{12} \,\mathrm{cm}^{-2})$  Si seems to rise even at 800°C [41]. As reported previously [32], the coordination number of Bi ion implanted Si  $(2.31 \times 10^{14} \,\mathrm{cm}^{-2})$  annealed at 600°C for 30 min was 1.1  $\pm$  0.5, which indicates that the most Bi atoms are not electrically activated. Furthermore, in

terms of the Bi-Si bond length, DFT calculations have shown that substitutional Bi, isolated or in a pair, compare well with experiment [32]. Therefore, we suggest that annealing at a high temperature causes vacancy mediated Bi diffusion, and eventually reconstruction of the local environment around the Bi atoms.

To study this effect more systematically, an additional sample was grown and unloaded from the chamber without any post-annealing. The sample was cut into small pieces, the surface layer removed, and then annealed at between 400 and 800°C for 30 min. As a control, the sample encapsulating 1 ML of Bi  $(2\times n)$  layer was also prepared (the Bi was deposited at 350°C and a Si cap layer was deposited at RT).

Corresponding carrier densities and mobilities were plotted as a function of annealing temperature in Fig. 5. As grown sample with Bi NLs showed  $p_{2D} - n_{2D} = +1 \times 10^{12} \,\mathrm{cm}^{-2}$ . In contrast to the samples with Bi NLs, the sample with Bi  $(2 \times n)$  1 ML showed  $p_{2D} - n_{2D} = -3 \times 10^{12} \,\mathrm{cm}^{-2}$ , indicating few Bi atoms are electrically activated and the density is larger than that of unintentional acceptors.

The sample with Bi NLs annealed at 400°C showed  $p_{2D}-n_{2D}\sim 10^{12}$  cm<sup>-2</sup>, which suggests that there was not enough SPE growth, and that Bi donors were not activated. By increasing the annealing temperature between 500-800°C, carrier densities reached  $p_{2D}-n_{2D}\sim 10^{14}$  cm<sup>-2</sup> at 500°C, then decreased monotonically. Meanwhile the mobility increased with decreasing carrier density. Whereas, the carrier density of the sample with Bi (2×n) did not change significantly, within the error bars.

There are two possible explanations for the change in carrier density of the sample with Bi NLs, either a decrease of donor density and/or an increase of acceptor density. Concerns over unintentional B contamination and an increase of their activation ratio were neglected since the Bi concentration is at least two orders of magnitude higher [12]. On the other hand, increasing vacancy-related defects may account for a decrease in donor density [42]. Donor-vacancy pairs of other Group V atoms, known as E-centres, are known to create a deep trap level near the middle of the Si band gap (P-V:  $E_c$  - 0.44 eV, Sb-V:  $E_c$  - 0.41 eV) [43]. These act as electron trap centres, without ionization, at room temperature. From an Arrhenius plot (n vs 1/T), the activation energy for the decreasing carrier density was calculated to be 0.5-0.6 eV. This is similar to the activation energy extracted from the diffusion process for Bi atoms. Thus, it is reasonable to suggest that at higher temperatures, some of the Bi donors will become deactivated through the creation of new Bi-V pairs.

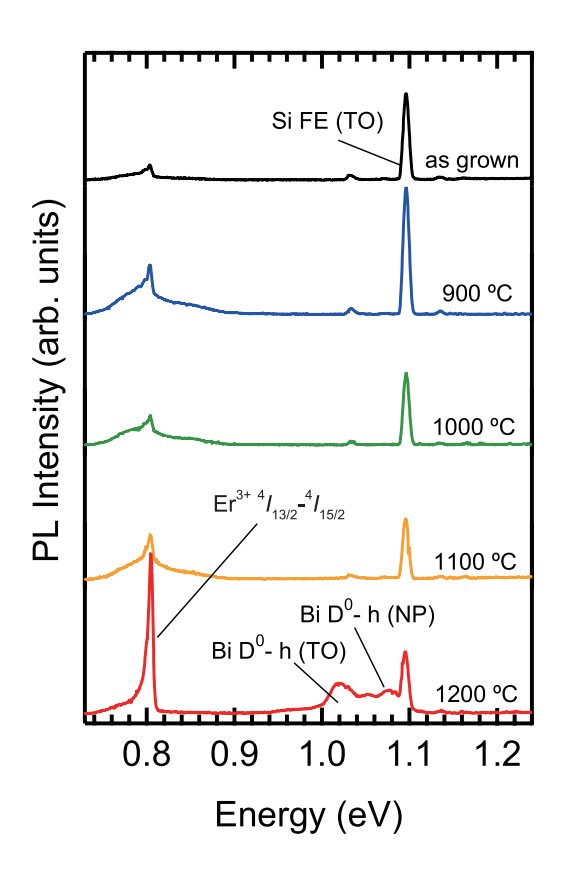


FIG. 6. Photoluminescence spectra of (Bi+Er)- $\delta$ -doped Si annealed by furnace at different temperatures. Deposited Er was 0.3 ML, Bi and Er densities determined by SIMS were  $5 \times 10^{12}$  and  $2 \times 10^{14}$  cm<sup>-2</sup>, respectively. Si FE (TO) denotes free exciton recombination in Si while Bi D<sup>0</sup>-h(TO) and D<sup>0</sup>-h(NP) denote TO- and non- phonon-mediated radiative recombination of an electron of a Bi donor with a free hole in Si. Er<sup>3+ 4</sup> $I_{13/2}$ -<sup>4</sup> $I_{15/2}$  denotes Er intra-shell transition.

Getting back to the Bi  $\delta$ -doped layer buried by Si crystal grown at around 400°C, it can be considered that Bi dopants are electrically activated in as-grown. Unfortunately, there is still little insight at this stage into the requirement for high temperature annealing to confirm the Bi donor bands by photoluminescence. One possible reason would be the existence of carrier traps near Bi dopants in as-grown  $\delta$ -doped layer, which obstructs the optical transition via Bi donor states, which might be related to crystal defects observed in TEM images. In this sense, high temperature annealing over 1100°C would be one of options when the defect-free sample is requested.

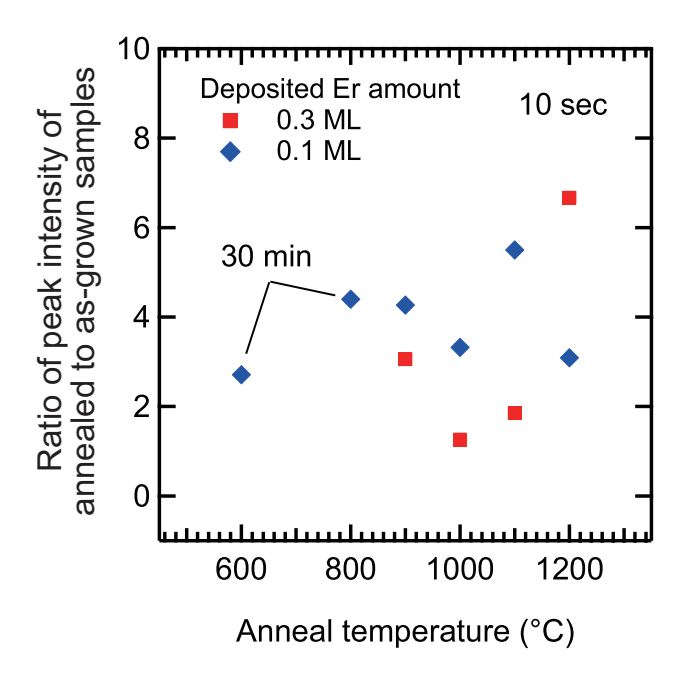


FIG. 7. Peak intensity ratio of Er intra-shell transition (Er<sup>3+</sup>  $^4I_{13/2}$ - $^4I_{15/2}$ ) as a function of annealing temperature. The samples were grown with 0.1 and 0.3 ML of Er. The luminescence peak intensified after annealing at temperatures around 1100 - 1200 °C for 10 sec.

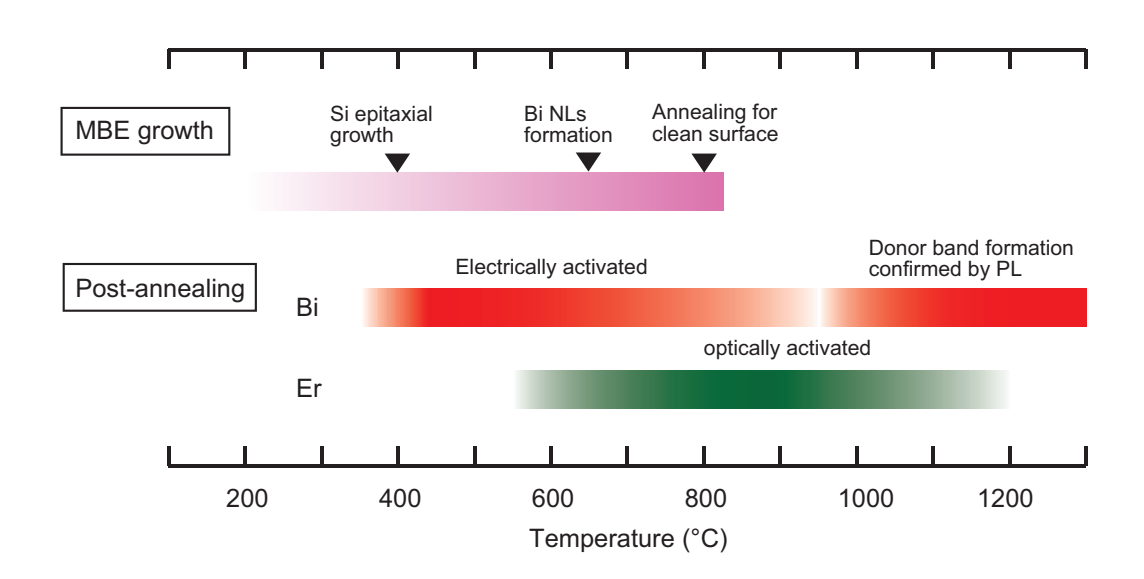


FIG. 8. Summary of process temperature for MBE growth to form  $(Bi+Er)-\delta$ -doped layer and subsequent post-annealing to activate both Bi and Er dopants in the layer.

## 2. Optically activated Er atoms

Figure 6 shows the photoluminescence spectra of (Bi+Er)- $\delta$ -doped Si (Bi and Er densities were  $5 \times 10^{12}$  and  $2 \times 10^{14}$  cm<sup>-2</sup>, respectively). The sample was grown with 0.3 ML of Er at 380°C without Bi surfactant. The deposited Er amount was tuned to suppress influence of unintentional luminescence peaks since highly concentrated (Bi+Er)- $\delta$ -doped samples tend to show dislocations-related peaks. From the as-grown sample, mainly luminescence peak related to Si free exciton recombination appeared with low Er-related luminescence. The post-annealing was performed in a furnace at various temperature for 10 s. The Er luminescence intensified after annealing at over 900°C. Annealing at 1200°C successfully developed luminescence peaks related to Bi D<sup>0</sup>-h and intensified the Er<sup>3+</sup> I<sub>13/2</sub>-I<sub>15/2</sub> luminescence.

Ratios of peak intensity of annealed to as-grown samples were plotted as a function of annealing temperature in Fig. 7. The data for a sample with 0.1 ML of Er (growth temperature of 340°C, without Bi surfactant) was also plotted. Annealing at 1100 and 1200°C gave the strongest peak for the samples with 0.1 and 0.3 ML of Er, respectively. The MBE-grown Si layer typically contains of the order of 10<sup>15</sup> cm<sup>-3</sup> O atoms, such that the O density might limit the activation ratio of Er atoms. In fact, when performing annealing at 1200°C for a longer time, the Er luminescence peak decreased for the sample with 0.3 ML. Note that laser annealing at close to the melting point of the Si crystal, which has been used for activation of Bi dopants [26], resulted in no luminescence peak related to Er dopants (not shown). It has been reported that a reason for decreasing luminescence intensity is the formation of Er clustering, as shown using atom probe tomography [44]. Therefore annealing at moderate temperature < 1200°C would be sufficient to activate Er atoms in (Bi+Er)-doped layer, but the optimized annealing condition would vary slightly.

# 3. Process temperature range for $(Bi+Er)-\delta$ -doped layer

Results in the subsections above showed that there is a suitable temperature for the activation of both Bi and Er dopants in Si. The temperature for post-annealing is summarized in Fig. 8, which includes specific temperatures during MBE growth. Since the optimized temperature for post-annealing would be varied by Bi and Er densities and the annealing duration, systematic studies are required to find out the optimized condition. Note that the

sample of the (Bi+Er)-doped layer with Er of 1 ML showed the dislocation-related peaks (D1) that hinder the Er luminescence peak.

The highest temperature during MBE growth is about 800°C, which is used to obtain the clean Si(001) surface. Thus it is possible to stack multiple  $\delta$ -doped layers with Si space layers by repeating the growth procedure while maintaining the quality of the Si surface. This enables not only more intense signals in photoluminescence studies but also the use of other experimental techniques such as DLTS (deep level transient spectroscopy) and ESR (electron spin resonance). Target densities of Bi and Er in a (Bi+Er)- $\delta$ -doped layer of  $\sim 10^{12}$  cm<sup>-2</sup> for QIPs [6], has been realized by the combination of MBE growth and subsequent annealing presented in this study.

#### IV. CONCLUSIONS

The (Bi+Er)- $\delta$ -doped layer in Si crystal was realized with use of Bi nanolines on Si(001) by molecular beam epitaxy. Bi and Er densities in the layer were controlled in the range of  $10^{12} - 10^{15}$  cm<sup>-2</sup> by the growth temperature for Si cap layer, the amount of deposited Er atoms (0.01 – 1 ML), and the coverage of Bi surfactant layer prior to the Si cap layer. Electrical activation of Bi dopants after annealing at 400–600°C were confirmed by transport measurement while the intensification of Er related luminescence peaks was observed after annealing at 600 – 1200°C. Subsequent post-annealing process is essential in this doping technique to activate both Bi and Er dopants in the  $\delta$ -doped layer.

#### ACKNOWLEDGMENTS

This work was supported by JSPS KAKENHI (20246017, 17H05225, and 17H02777 to K. Miki, 20121355 to K. Murata, 16H05895 and 17KK0127 to S. Yagi) and the NIMS Nanofabrication Platform in the Nanotechnology Platform Project from the Ministry of Education, Culture, Sports, Science and Technology, Japan (MEXT). Calculations were performed using the UCL Legion High Performance Computing Facility, and associated support services. C. J. Kirkham was funded through a UCL Impact Studentship. This experiment is based on the results at the beamlines BL37XU, BL25SU and BL13XU, SPring-8 with the approval of Japan Synchrotron Radiation Research Institute (JASRI) (Proposal

Nos. 2011B1692, 2012A1546, 2012B1664, 2016A1373, 2017B1248, 2018B1178, 2018B1179, and 2018B1198). We give acknowledgement to Dr. K. Nitta, Dr. T. Uruga, Dr. Y. Terada, Dr. T. Muro, and Dr. H. Tajiri and JASRI/ SPring-8 for technical help and discussion of the results. We give acknowledgement to Dr. Nitta, Dr. Uruga and Dr. Terada, and JASRI/ SPring-8 for technical help and discussion of the results. Regarding the mechanism of surface segregation and the photoluminescence related Er, we would like to acknowledge to Dr. Yasutake and Prof. Fukatsu in the University of Tokyo. We also would like to acknowledge to Dr. Sakamoto in National Institute of Advanced Industrial Science and Technology (AIST) for MBE growth.

### DATA AVAILABILITY STATEMENT

The data that support the findings of this study are available upon reasonable request from the authors.

<sup>[1]</sup> J. Zhang, K. Tse, M. Wong, Y. Zhang, and J. Zhu, Frontiers of Physics 11, 117405 (2016).

<sup>[2]</sup> S. Yuan, X. Yu, D. Hu, H. Luo, X. Zhu, Y. Xu, L. He, H. Chen, and D. Yang, Solar Energy Materials and Solar Cells 203, 110189 (2019).

<sup>[3]</sup> K. Miki, H. Matsuhata, K. Sakamoto, G. A. D. Briggs, J. H. G. Owen, and D. R. Bowler, Inst. Phys. Conf. Ser. 164, 167 (1999).

<sup>[4]</sup> G. W. Morley, M. Warner, A. M. Stoneham, P. T. Greenland, J. v. Tol, C. W. M. Kay, and G. Aeppli, Nat. Mater. 9, 725 (2010).

<sup>[5]</sup> J. J. L. Morton, A. M. Tyryshkin, R. M. Brown, S. Shankar, B. W. Lovett, A. Ardavan, T. Schenkel, E. E. Haller, J. W. Ager, and S. A. Lyon, Nature 455, 1085 (2008).

<sup>[6]</sup> A. M. Stoneham, A. J. Fisher, and P. T. Greenland, J. Phys. Condens. Matter 15, L447 (2003).

<sup>[7]</sup> B. M. Hudak, J. Song, H. Sims, M. C. Troparevsky, T. S. Humble, S. T. Pantelides, P. C. Snijders, and A. R. Lupini, ACS Nano, ACS Nano 12, 5873 (2018).

<sup>[8]</sup> K. Miki, J. H. G. Owen, D. R. Bowler, G. A. D. Briggs, and K. Sakamoto, Surf. Sci. 421, 397 (1999).

- [9] J. H. G. Owen, F. Bianco, S. A. Koster, D. Mazur, D. R. Bowler, and C. Renner, Appl. Phys. Lett. 97, 093102 (2010).
- [10] K. Murata, K. Miki, and S. Fukatsu, Appl. Phys. Lett. 111, 152104 (2017).
- [11] J. H. G. Owen, K. Miki, and D. R. Bowler, J. Mater. Sci. 41, 4568 (2006).
- [12] K. Miki, K. Sakamoto, and T. Sakamoto, Surf. Sci. 406, 312 (1998).
- [13] S. Yagi, W. Yashiro, K. Sakamoto, and K. Miki, Surf. Sci. 595, L311 (2005).
- [14] P. Hohenberg and W. Kohn, Phys. Rev. **136**, B864 (1964).
- [15] W. Kohn and L. J. Sham, Phys. Rev. **140**, A1133 (1965).
- [16] G. Kresse and J. Hafner, Phys. Rev. B 48, 13115 (1993).
- [17] G. Kresse and J. Furthmüller, Phys. Rev. B **54**, 11169 (1996).
- [18] P. E. Blöchl, Phys. Rev. B 50, 17953 (1994).
- [19] G. Kresse and D. Joubert, Phys. Rev. B **59**, 1758 (1999).
- [20] J. Perdew, K. Burke, and M. Ernzerhof, Phys. Rev. Lett. 77, 3865 (1996).
- [21] G. Henkelman, B. Uberuaga, and H. Jonsson, J. Chem. Phys. 113, 9901 (2000).
- [22] K. Miyashita, Y. Shiraki, D. C. Houghton, and S. Fukatsu, Appl. Phys. Lett. 67, 235 (1995).
- [23] K. Sakamoto, K. Kyoya, K. Miki, H. Matsuhata, and T. Sakamoto, Jpn. J. Appl. Phys. 32, L204 (1993).
- [24] H. Matsuhata, K. Sakamoto, and K. Miki, J. Electron Microsc (Tokyo) 53, 325 (2004).
- [25] S. M. Sze and K. K. Ng, *Physics of Semiconductor Devices*, 3rd ed. (Wiley-Interscience, 2006).
- [26] K. Murata, Y. Yasutake, K. Nittoh, K. Sakamoto, S. Fukatsu, and K. Miki, Appl. Phys. Express 3, 061302 (2010).
- [27] S. Coffa, F. Priolo, G. Franzo', V. Bellani, A. Carnera, and C. Spinella, Phys. Rev. B 48, 11782 (1993).
- [28] Y. Shimizu, Y. Tu, A. Abdelghafar, M. Yano, Y. Suzuki, T. Tanii, T. Shinada, E. Prati, M. Celebrano, M. Finazzi, L. Ghirardini, K. Inoue, and Y. Nagai, in 2017 Silicon Nanoelectronics Workshop (SNW) (2017) pp. 99–100.
- [29] A. Taguchi and K. Takahei, J. Appl. Phys. **79**, 4330 (1996).
- [30] A. J. Kenyon, Semiconductor Science and Technology 20, R65 (2005).
- [31] N. A. Sobolev, O. B. Gusev, E. I. Shek, V. I. Vdovin, T. G. Yugova, and A. M. Emelyanov, Applied Physics Letters **72**, 3326 (1998).

- [32] K. Murata, C. Kirkham, M. Shimomura, K. Nitta, T. Uruga, Y. Terada, K. Nittoh, D. R. Bowler, and K. Miki, Journal of Physics: Condensed Matter 29, 155001 (2017).
- [33] G. Olson and J. Roth, Materials Science Reports 3, 1 (1988).
- [34] J. Song, B. M. Hudak, H. Sims, Y. Sharma, T. Z. Ward, S. T. Pantelides, A. R. Lupini, and P. C. Snijders, Nanoscale 10, 260 (2018).
- [35] Y. Ishikawa, K. Yazaki, and I. Nakamichi, Jpn. J. Appl. Phys. 28, 1272 (1989).
- [36] H. Bracht, MRS Bulletin, **25**, 22 (2000).
- [37] C. Jacoboni, C. Canali, G. Ottaviani, and A. A. Quaranta, Solid-State Electronics **20**, 77 (1977).
- [38] R. Duffy, T. Dao, Y. Tamminga, K. van der Tak, F. Roozeboom, and E. Augendre, Appl. Phys. Lett. 89, 071915 (2006).
- [39] J. Narayan and O. W. Holland, phys. stat. sol. (a) 73, 225 (1982).
- [40] J. P. De Souza and P. F. P. Fichtner, J. Appl. Phys. **74**, 119 (1993).
- [41] C. D. Weis, C. C. Lo, V. Lang, a. M. Tyryshkin, R. E. George, K. M. Yu, J. Bokor, S. a. Lyon, J. J. L. Morton, and T. Schenkel, Appl. Phys. Lett. 100 (2012).
- [42] G. D. Watkins, Materials Science in Semiconductor Processing 3, 227 (2000).
- [43] M. Mamor, M. Elzain, K. Bouziane, and S. H. Al Harthi, Phys. Rev. B 77, 035213 (2008).
- [44] E. Talbot, R. Lard, P. Pareige, L. Khomenkova, K. Hijazi, and F. Gourbilleau, Nanoscale Research Letters 8, 39 (2013).